Depth distribution of particles in plastics in sea-water

Nicolò Tuccori
nicolo.tuccori@tecnico.ulisboa.pt

Instituto Superior Técnico, Lisboa, Portugal

September 2018

Abstract

Plastic becomes a persistent contaminant in aquatic systems. The adherence of abiotic and biotic materials to plastics may potentiate structural changes and their degradation. How the main elements present in sea water interact with polymers is largely unknown. Nuclear microprobe clusters PIXE and RBS techniques, which offer unique possibilities to characterize the materials deposited on the surface of plastics rejected to the aquatic environment. These techniques enable to study penetration profiles of elements that are present in the deposits, estimate their depth structure and polymer matrix variations. Food packaging polymers, high-density polyethylene (HDPE) and polyethylene terephthalate (PET) exposed to turbid water of the Tagus estuary were studied. The deposition mosaic contained clastic, biota and saline components. A major finding was the diffusion of the ion Cl^- in the polymer matrix. This was possible by examining elemental profiles taken in transversal sections of the polymers. The depth structure of deposits was estimated using RBS and PIXE data applying general purpose programs, such as OMDAQ2007 and NDF. To illustrate the capabilities of these analytical tools the depth structure of biotic and abiotic deposits was examined. The results pointed out for a multilayer depth structure which can decode the complex arrangement of cellular and sedimentary materials deposited on the polymers surface. In addition, it was possible to identify sources of uncertainties in simulating the interface and the changeable polymer matrix in deeper regions.

Keywords: OMDAQ2007, WiNDF, depth structure, PET, HDPE, aquatic contamination

1. Introduction

Increasing amounts of floating plastic debris in rivers, estuaries and sea is a preoccupying environmental and toxicological issue [1]. Over time, plastics break down into smaller pieces due to weathering, such as sunlight exposure, oxidation, waves action, currents, and grazing forming particles with less than 5 mm, the so called microplastics [2]. It is currently consensual that the adherence of biota and inorganic suspended particles as well as soluble materials to plastics, eventually interact with polymers favouring their structural changes, degradation and fragmentation [3]. However, how abiotic (earth crust materials and saline compounds) and biotic materials in water interact with the polymers and promote their ageing process is still an open question. Recent studies point out for a possible absorption of earth crust materials by the polymer, which may be dependent on the plastic chemical nature [4]. Other possible process involves adherence of clastic materials to plastics increasing oxidized moieties, that in turn facilitate the adhesion of microorganisms. These synergistic events persist through time leading to a relatively steady film covering the plastic material, which may favour the weathering of the surface of the polymer. Measurements of chemical elements deposited on plastics at a microscale are virtually lacking. Especially, how major ions present in sea water, e.g., Cl, Na, S, Ca, K, Br, interact with polymers is largely unknown. Microbeam capabilities offer unique possibilities to characterize the complex deposits on the surface of daily use plastics, which are rejected to the environment. Nuclear microscopy, which mainly clusters PIXE and RBS techniques together with ion beam analytical tools, such as OMDAQ2007 and NDF, enables to characterize the depth structure of the deposits and assess the depth distribution of elements in the deposit and inside the polymer matrix [5]. This will help reconstructing a 3-dimentional picture of the deposits and characterize polymer matrix changes. The objective of this study is thus to examine the elemental composition of deposits in plastics exposed to a turbid estuarine environment and to learn about the depth penetration of key elements into the plastics.

2. Background

In this experimental work, the analysis of the plastic samples are provided by the simultaneous collection of PIXE and RBS events. Considered singularly, each of these techniques permits the characterization of materials, with different features and results.

2.1. Particle-Induced X-ray Emission (PIXE)

PIXE is based on the excitation of inner-shell electrons from target atoms by the energetic incident particle impact and the spectroscopy of the subsequently emitted X-rays during the electronic relaxation. The counts on the PIXE spectrum related to the X-rays emitted by the element Z (atomic mass A) is called *yield* $Y_P(Z)$. To estimate the elemental concentration N_z $(atoms/cm^3)$ of the element in the sample, precise knowledge of the ionization cross section $\sigma_z(E)$, of the fluorescence yields ω and of branching ratios b is required. Furthermore, for thick targets, the overall stopping power of the sample matrix $S_M(E)$ and, if there are absorbers, the transmission coefficient t, have to be known. For the geometry shown in Fig.1, with a homogeneous

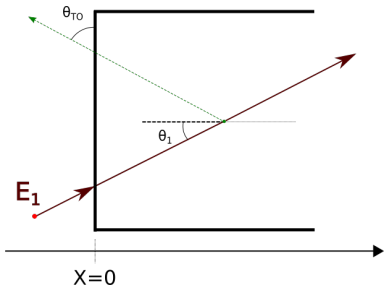

Figure 1: Scheme of PIXE experimental geometry.

sample of intermediate thickness, the concentration of a specific element can be estimated from the elements PIXE yield, with the equation [6]:

$$Y_P(Z) = \omega\ b \cdot N_z \cdot G_P(Z) \cdot \int_{E_1}^{E_f} \frac{\sigma_z(E) T_z(E)}{S_M(E)} dE \qquad (1)$$

Here, considering a general experimental setup, E_1 is the initial ion energy, and E_f, is the final energy on exit from the sample. $G_P(Z)$ is an experimental parameter,

$$G_P(Z) = \epsilon_P(E_Z) \cdot \frac{\Omega_P}{4\pi} \cdot N_p \cdot (1 - DTR_P) \cdot t$$

where Ω_P is the detector solid angle, $\epsilon_P(E_Z)$ is its relative efficiency, E_Z the emitted X-ray energy, DTR_P the detector dead time ratio and N_p is the number of incident protons. The quantity $T_z(E)$ describes the X-ray transmission from the successive depths in the matrix.

2.2. Rutherford Backscattering Spectroscopy (RBS)

The fundamental basis of RBS is the detection and analysis of the projectile ions which are backscattered after the interaction with the target nuclei that compose the sample matrix. Measurements of the number and energy distribution of these ions, provide the quantitative determination of the composition of a material and depth profiling of individual elements. The theoretical scattering model that describes this technique raise from the assumption that the process is a two-body elastic collision between two isolated particles of masses M_1 and M_2. The incident particle with mass M_1, atomic number Z_1 and energy E_1, interacts with a nucleus of the sample, at rest in the laboratory frame ($E_2 = 0$), with mass M_2 and atomic number Z_2. After the scattering process, the projectile is deflected at an angle θ with kinetic energy $E_1{}'$ while the target nuclei is scattered through the recoil angle Φ with kinetic energy $E_2{}' \neq 0$. The energy $E_1{}'$ of the scattered projectile ion is determined by applying conservation of kinetic energy and of longitudinal and transverse momentum of the two-body system after the scattering process. Using the related equation, considering $M_1 < M_2$, it is possible to define the *Kinematic factor* K_{target} as the ratio between the energy before and after the interaction:

$$K_{target} = \frac{E_1{}'}{E_1} = \left[\frac{\sqrt{1-(M_1/M_2)^2 \sin^2\theta} + (M_1/M_2)\cos\theta}{1+(M_1/M_2)} \right]^2 \qquad (2)$$

As highlighted by the subscript, this factor has an intrinsic dependence on the target element. Hence, for a ion with known light mass M_1 (e.g. ^1H or ^4He), the energy loss of the incident ion, after elastically colliding with the target atom, becomes a function only of the scattering angle θ and the target mass M_2. Therefore, the kinematic factor permits to recognize the element of the sample involved in the scattering process (given that the collision happens in the sample surface).

The capability of characterizing the analyzed sample in depth rely mainly on the energy loss of the analysis beam ions as they traverse the specimen. The *stopping power* of a material is usually defined as the energy loss per distance travelled by a particular ion in the material and is denoted as dE/dx. It includes two contributions, the electronic and the nuclear scattering processes. In RBS applications, MeV light ions beam are used and the rate of the electronic energy loss can be characterize by the *Bethe-Block* formula in the non relativistic approximation [7]:

$$-\left.\frac{dE}{dx}\right|_e = \frac{4\pi}{m_e} \cdot \frac{n_e {Z_1}^2}{{v_1}^2} \cdot \left(\frac{e^2}{4\pi\epsilon_0}\right)^2 \cdot \ln\left(\frac{2m_e {v_1}^2}{I}\right) \qquad (3)$$

where v_1 is the projectiles velocity, n_e the number

of electrons per unit volume, m_e the electron mass and I the mean excitation potential. The beam ions are characterized by their dE/dx, that, considering the in and out-coming trajectories of the particles, enables the extraction of depth information from the sample. Figure 2 schematize the backscattering process.

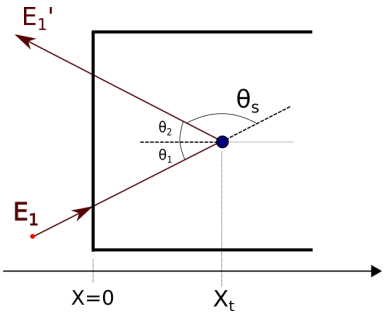

Figure 2: Scheme of a backscattering event at a certain depth in the sample.

The particle enters in the sample with an energy E_1 and an angle θ_1 respect to the surface normal. After having transvered a depth x_t in the material, it is backscattered at an angle θ_s, losing a fraction of its energy, given by the kinematic factor. In order to be detected and contribute to the RBS spectrum, it then goes through the sample until it emerges off at an angle θ_2 respect to the normal of the sample surface. The ion loses an energy ΔE_{in} along its path into the sample and ΔE_{out} along its path out of the sample, where

$$\Delta E_{in} = \int_0^{x_t/\cos\theta_1} \left.\frac{dE}{dx}\right|_{E_1} dx \qquad \Delta E_{out} = \int_{x_t/\cos\theta_2}^{0} \left.\frac{dE}{dx}\right|_{E_s} dx \qquad (4)$$

in which the subscripts E_1 and E_s stand for the energy value from which the energy loss has to be evaluated. The first is the ion energy before entering the sample while E_s is its energy just after being scattered, $E_s = K_{target}(\theta_s)\cdot(E_1 - \Delta E_{in})$, where $K_{target}(\theta_s)$ is the kinematic factor given in Eq. 2, that depends directly on the backscattered angle θ_s and the target atom. The measured backscattered ion energy $E_1{}'$ from a given element at a depth x_t is thus

$$E_1{}' = K_{target}(\theta_s)\cdot(E_1 - \Delta E_{in}) - \Delta E_{out} \qquad (5)$$

Using the proper rates of ion energy loss and kinematic factors, the energy spectrum of the collected backscattered ion can be converted to the depth profile of each element of the sample.

The RBS technique enables also the determination, with considerable precision, of the stoichiometry of the sample elemental matrix. Considering a uniform beam of normal incidence on an uniform sample surface, the numbers of backscattered ions detected after interacting with a layer of atoms with mass A of thickness Δt, uniformly distribuited with concentration N_A, is given by:

$$Y_R(A, \Delta t, \theta_s) = G_R \cdot N_A \cdot \int_0^{\Delta t} \sigma_R(E(x_t), \theta_2) dx_t \qquad (6)$$

where $\sigma_R(E(x_t), \theta_2)$ is the scattering cross section at angle θ_2 evaluated at ion energy $E(x_t)$, with x_t the depth of the involved target atom and $G_R(Z)$ the experimental parameter related to the RBS setup:

$$G_R = \frac{\Omega_R}{4\pi} \cdot N_p \cdot (1 - DTR_R)$$

Using beam energies typically in the order of few MeV, the scattering cross section can be assumed to be the Rutherford. N_p is the measured number of incident particles, DTR_R the detector dead time ratio and Ω_R its solid angle. Eq. 6 can be efficiently used if in the spectrum, the full peak of the considered element can be resolved, so that the element concentration N_A can be estimated.

2.3. PIXE and RBS complementarity

IBA techniques, together with the characteristic features present also limitations. For PIXE, when analyzing a thick sample, the elemental composition of the matrix is required to estimate the concentration of the elements. If this is not known, precise information can not be deduced. On the other hand, RBS analysis are not fruitful when they have to deal complex structure samples, being either multi-elemental or multi-layered or even both. In these situations, the multiple variables that have to be considered, originate ambiguities in the RBS spectrum interpretation and, as a result, there is not a unique matrix that simulates properly the spectrum.

These limitations can be partially solved by clustering the two techniques. The analysis provided singularly, in fact, focuses in different features of the sample. As such, combining the data, complementary and self-consitent results can be obtained. In particular, for PIXE and RBS, two different approaches are possible. The first consists in improving the PIXE estimation of the elements concentrations in a thick sample using the RBS capability of estimate the sample matrix and provide a correction to the measured charge, that may differ from the effective one. This method is called *Q-factor*, from the charge correction parameter [8]. Vice versa, the RBS depth profiling evaluation can be improved limiting the possible matrices that fits the spectrum to the ones that produce also a PIXE simulation that is in agreement with the related data [9].

3. Experimental Analysis

Food packaging polymers, such as high-density polyethylene (HDPE) and polyethylene terephthalate (PET) were exposed to turbid water of the

Tagus estuary for 30 days. Pieces of these polymers of approximately of 2.5 x 5 cm^2 were used and suspended in the water-column at the same depth. After exposure, samples retrieved from the site were air dried. Pieces of approximately 0.5 cm^2, representative of high and low deposition areas, were cut for further nuclear microscopy analysis. For precise and clean cuts a surgical blade was used. Pristine samples were used as controls. The polymer materials were analysed at the nuclear microprobe facility of IST/CTN [10]. A proton beam of 2.0 MeV and 100 pA current focused to a 3 x 4 μm^2 spot size was used. PIXE and RBS analysis were carried out simultaneously to assess the micro-distribution maps of elements on the surface (surface analysis) and in cross sections (transversal analysis) of the samples. Linescans were also obtained in selected regions of transversal sections. Acquisition of data was performed using OMDAQ (Oxford Microbeams Ltd, UK). The polymer samples were mounted on a sample stage with a goniometer that enabled the positioning of the samples to produce elemental mapping of the surface deposits and of the transversal sections of the polymers. The polymer samples were carbon coated to avoid charge build up. The analysis of PIXE and RBS data obtained in surface mapping and transversal profiles was carried out using software analytical tools such as, i) OMDAQ2007 (Oxford Microbeams Ltd, UK), which provides an interface for GUPIX [11] and RUMP [12], to estimate the charge and the matrix through the RBS spectra to normalize PIXE data, and produce quantitative elemental measures; ii) NDF to define a high-resolution depth structure of the deposit and changes of the polymer matrix at the interface. NDF uses complementary data from PIXE spectra collected simultaneously to generate a single solution consistent with the RBS depth profile as fit parameter. The program calculates the PIXE elemental yields for the layer structure that best fit the RBS spectra comparing them to the elemental yields in the PIXE spectra obtained experimentally. In both OMDAQ2007 and NDF approaches the depth profile is represented by finite layers with constant concentrations.

4. Results

4.1. Surface elemental distribution

In both HDPE and PET the deposition mosaic consisted of abiotic and biotic components. The deposits showed saline, sediment-like materials and a large diversity of organisms dispersed in a non-homogeneous manner and arranged in a complex layered distribution, as can be depicted in Figure 3.

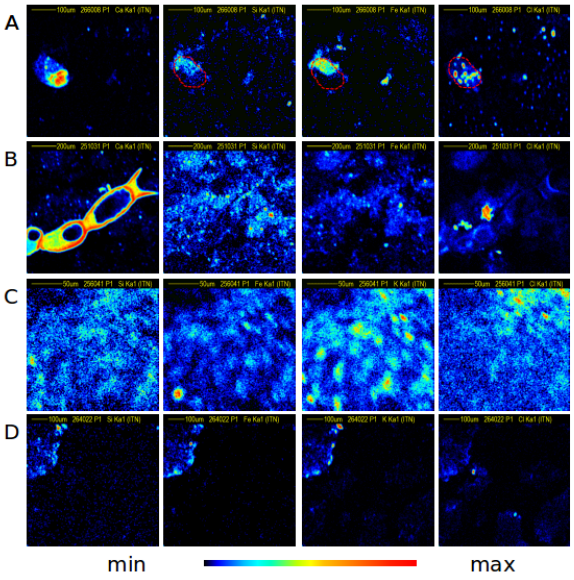

Figure 3: Elemental distribution of several surface deposits.

Biota can be easily identified through the Ca map, as calcium carbonate is the building block for the cell walls, shells and skeletons of many marine organisms. Marine organisms are intertwined with sedimentary materials that can be inferred by Si, Fe and K, and saline deposits such as Cl (see Figure 3-A and B) even when cells are isolated in regions with very low deposit (Figure 3-A). This distribution pattern suggests an association of biota with sedimentary materials that may stabilize the adhesion to the polymer substrate. Concerning sedimentary materials, a variety of grain sizes was observed, probably silt, clay or other earth crust materials (e.g., Si, Ti, Fe, K and Ca) and salt particles (e.g., Cl) (Figure 3-C). These elemental signatures are also present in regions of the plastics with very low deposits (Figure 3-D). However, the distribution of Cl followed a different pattern of the other elements that characterize the sedimentary material. This was also evident in panels A and B of Figure 3, where Cl particles that populate the deposit regions showed well defined boundaries likely crystals of sea salt and were not correlated with major sedimentary grains or cells.

4.2. Transversal elemental distribution

The polymer matrices and deposits were also inspected by transversal analysis. By rotating the samples of 90°, the cross section of the polymer could be scanned and line profiles produced in regions of interest. These line profiles were taken in both pristine (control) and exposed samples. In the latest, high-loaded regions, low-loaded regions and virtually clean regions of the plastic sample were

examined. The number of counts for each element in the PIXE and RBS spectra was plotted in function of depth. Only one edge was analysed at a time, due to the system geometry. The results obtained for the pristine polymers, showed that PET is a very uniform material (Figure 4 A, B and C).

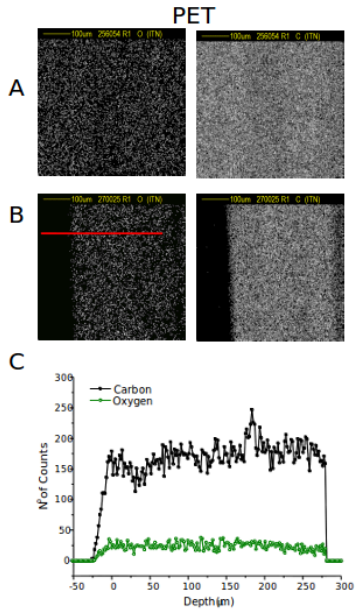

Figure 4: Transversal section analysis of PET pristine samples: maps and linescans.

The HDPE polymer used in the study contained Ti homogeneously distributed in the C matrix and Ca in a grain like structures (Figure 5 D and E). These features can be clearly inferred in surface and transversal analysis and in elemental profiles (Figure 5 D and F).

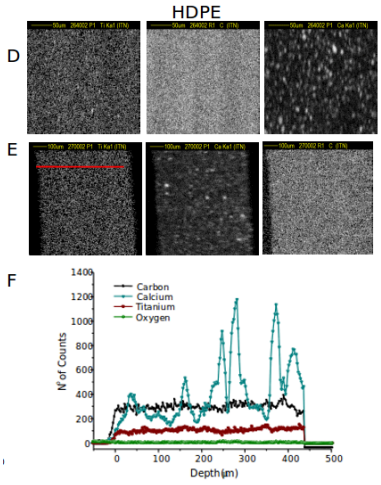

Figure 5: Transversal section analysis of HDPE pristine samples: maps and linescans.

In Figure 6 cross section analyses of PET and HDPE samples of a high-load deposit region are displayed.

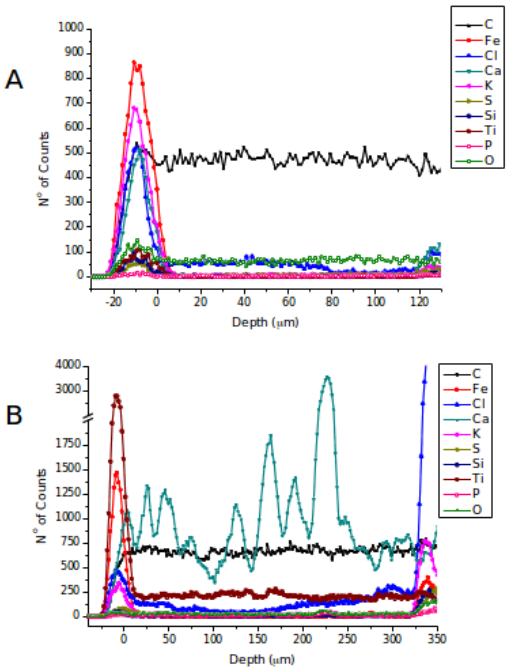

Figure 6: Linescans of exposed samples showing several elements.

The selected cases illustrate the profiles of elements detected in the PIXE and RBS spectra in the polymers cross section. The plastic surface was set visually by the user using the C signal from RBS spectra to define the edge of the polymer. This boundary was taken as the zero depth. The elemental distributions showed that deposits can be easily identified by well-defined peaks of several elements (e.g., Si, K, Ca, Ti, Fe) in front of the substrate edge. The elemental profiles of polymers cross-sections enabled to have an estimation of the deposit thickness. A Gaussian fit of the peaks of individual elements provided a consistent estimation of the width of the deposit in each sample. For the line scans plotted in Figure 6, the deposit widths were of 9-15 μm in PET and 14-18 μm in HDPE. However, the calculated deposit width is just indicative and comparison between samples not straightforward.

A relevant Cl diffusion in the polymer matrix was observed in both PET and HDPE (see Figure 6 A and B). However, the Cl diffusion into the plastic was largely nonhomogeneous. In some regions a relevant diffusion occurred whereas others are devoid of Cl, as illustrated by the images of the transversal sections of both polymers in Figure 7.

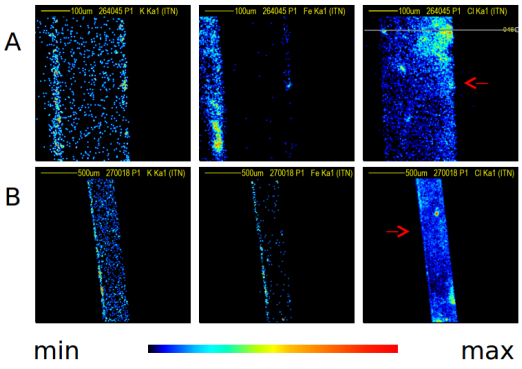

Figure 7: Transversal section maps of different samples that present Cl diffusion.

There was no evidence of diffusion for any other element detected. This procedure had limitations in what concerns assessing penetration profiles at the deposit-polymer interface. The major limitations were imposed by the lateral resolution of the beam and the demarcation of the polymer boundary defined visually by the user. Nevertheless, the surface and transversal characterization of the polymers enabled us (i) to associate elemental composition with sedimentary deposits and identify biological colonization of the plastic surface, (ii) to evaluate the magnitude of the thickness of the deposits, and (iii) to establish elemental profiles which permitted to identify the nonhomogeneous diffusion of Cl in both polymer matrices.

4.3. Evaluation of depth structure of deposits

The cross-section analyses of the polymers did not provide information about the structure of the deposits, despite important information about the elemental composition of those deposits and the spreading of Cl inside the polymers matrix. Besides, the manipulation of the sample may create artefacts as particles of the deposit can be dragged or splashed to the cross section during cut. Also, transversal analysis of thin plastics ($< 100\ \mu m$) will be demanding. Therefore, it is important to translate the results obtained in transversal analysis to surface analysis. This is possible by using RBS data of surface analysis and ion beam tools such as OMDAQ2007 and NDF programmes that will enable to estimate the structural composition of the deposit and to examine the deposit-polymer interface and the changes of the polymer matrix. The rationale of using RBS data of surface analysis is the better depth resolution achieved with RBS in comparison to PIXE for the transversal profiles, which is limited by the beam lateral resolution. The approach was applied to spectra collected in two types of deposits on PET and HDPE, such as biological and sedimentary materials. These spectra corresponded to point analysis from details identified in surface analysis maps, i.e., tiny areas equivalent to the beam dimensions (approximately 3 x 4 μm^2). The polymer matrix was first estimated using the RBS spectra of pristine polymers and included in OMDAQ2007 and NDF analysis of deposits as a substrate layer. The HDPE matrix estimation using both OMDAQ2007 and NDF produced the same result (C 99 % + (Ca+Ti) 1 %); thickness $>300\mu m$), whereas the PET matrix was marginally different when OMDAQ2007 results (C 67 % +O 33 % using; thickness $>100\ \mu m$) were compared to NDF results (C 77 % + O 23 %; thickness $>100\ \mu m$). The OMDAQ2007 result of the RBS fit was consistent with the PET stoichiometry ($C_{10}H_8O_4$). The NDF result was influenced by the lack of relevant elements detectable by PIXE. Only Ca (probably present as an impurity) was used in the NDF calculations and the very low statistics of the peak lead to a less adjusted solution.A three-layer structure was initially assumed for the two types of deposits: (i) the thin carbon coating used to avoid charge build up during irradiation; (ii) the deposit layer based on major elements that can be detected in both RBS and PIXE spectra; and (iii) the fixed substrate layer, the polymer matrix. The OMDAQ2007 output gives the best RBS spectra fit based on the user initial guess of the layer structure, elemental composition and thickness of each layer. Improvements can be obtained by adjusting elemental composition in each layer, beam energy and RBS detector resolution. The fit results obtained for a detail of a cell adherent to HDPE, corresponding to the cell wall and a sedimentary deposit on PET is displayed in Figure 8.

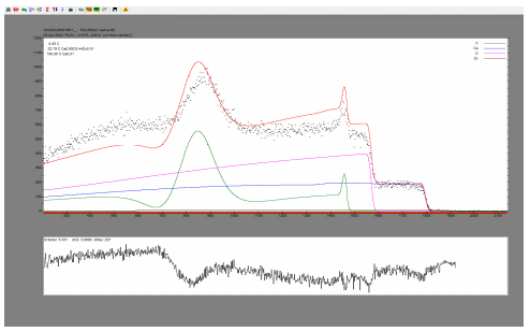

Figure 8: RBS spectrum of a point analysis in a cell wall.

The first layer reproduced the thin C film at the surface (C 100 %; thickness = 0.08 μm) and the second layer was consistent with biological material composition and thickness (C 19.4 % + O 66.9 % + Ca 13.4 % + Zn 0.2 %; thickness = 22.8 μm). The substrate layer was the simulated HDPE matrix as referred above. Likely, the sediment region RBS

spectrum fit can be seen in Figure 9.

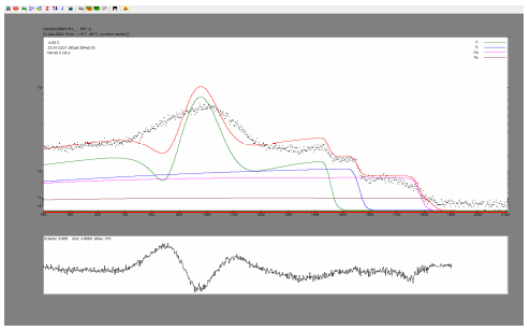

Figure 9: RBS spectrum of a point analysis in a sedimentary deposit area.

The first layer reproduced the thin C film at the surface (C 100 %; thickness = 0.05 μm), the second layer was consistent with sedimentary material composition (C 53 % + O 37 % + Ca 9.2 % + Fe 0.8 %; thickness 23.3 μm), and the third layer corresponded to the PET matrix (Figure 9). However, OMDAQ2007 did not reproduce the shape of the resonance very well nor the shape of the barriers of heavier elements in the spectra. The results obtained point out that a more complex matrix structure may be required, which has to be defined manually when using OMDAQ2007. If this multilayer structure will have common elements in each layer, it will imply that the OMDAQ2007 capability of calculating elemental concentrations using PIXE spectra can only be performed in a single layer, as total multilayer quantitative analysis is only possible if layers do not share the same element(s).

NDF can estimate a multilayer composition and thickness that best describe the sample with the best possible accuracy departing from an initial guess defined by the user (e.g., OMDAQ2007 best fit). The deposit thickness, number of layers and matrix composition was then estimated by adjusting beam energy, detector resolution, RBS and PIXE charge and combining relevant elements in both RBS and PIXE spectra. Thus, elemental concentrations can only be calculated for the elements that are detected both by PIXE and RBS. The NDF generates a single solution consistent with the RBS depth profile as fit parameter and PIXE elemental yields. The NDF simulation of the RBS spectra of the cell detail on HDPE provided an interesting solution for the depth structure described by four layers, which is meaningful in terms of cellular morphology. The quality of the fit was evident and the agreement between the experimental PIXE yields and those calculated for the sample structure fitted was also very good (Figure 10 A and B).

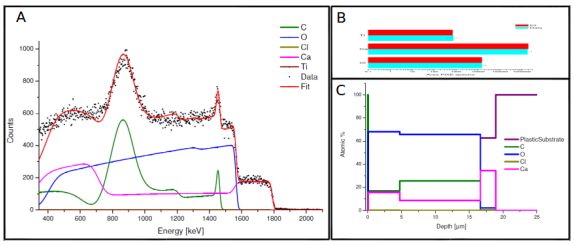

Figure 10: NDF analysis of point data of a cell wall.

Apart the first thin C coating layer (as obtained in OMDAQ2007 approach), the second layer composition (C 16 % + O 68 % + Ca 16 %) reproduced the atomic percentages in calcium carbonate ($CaCO_3$) a major constituent of the cell wall of many marine organisms, and the third layer, showed a composition closer to an intracellular milieu, less Ca, more C and O (C 26 % + O 66% + Ca 9%). The fourth layer was noteworthy as it reveals a mixed composition of the cell wall and the polymer (C 0.2 % + O 2.2 % + Cl 0.4 % + Ca 34 % + substrate 63 %). This mixed composition is compatible with the required cell adhesion to the substrate (the 5^{th} layer HDPE) and may reflect the biodegradation of the polymer surface carried out by enzymatic hydrolysis of specific polymer bonds. The layer structure and the relative elemental composition of each layer can be represented by plotting the fitted depth profile derived from the RBS data with the linear depth scale as in Figure 10 C. The results obtained with NDF for the sedimentary material, evidenced the high complexity of the deposit that could be already guessed from the unsatisfactory OMDAQ2007 result. The simulation delivered a depth structure of 8 layers with different thicknesses and composition, compatible with a mixture of organic matter and earth crust materials. This structure reproduced the spectra shape accurately. The calculated PIXE yields for Si, Cl, K, Ca and Fe showed also a remarkable agreement with the experimental data (see Figure 11 A and B).

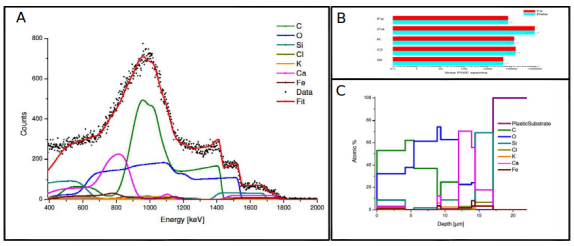

Figure 11: NDF analysis of point data of a mixed deposit region.

The depth structure evidenced a larger organic contribution at the deposit surface (higher C atomic percentage in the first three layers) and more oxi-

dized Fe, Ca and Si earth crust materials deeper in the deposit. Interestingly, Cl was also present at deeper layers, suggesting proximity of the substrate that may favour its diffusion into the polymer matrix (Figure 11 C). The Cl^- ions, a major ion in seawater, may have an important role of in plastic degradation that is still not fully elucidated. However, due to the low yield of the elements of interest relative to matrix it was not possible to model the diffusion of Cl or any other element in the matrix. To assess matrix changes the element yield should overcome the uncertainty of the fit of the upper layers and the matrix. Beam straggling in upper layer of the deposit and attenuation of the incoming energetic particles by the materials in the deposit also limit the analysis capacity in the evaluation of polymer-deposit interaction and matrix changes.

5. Conclusions

To our knowledge, the reported results were the first measurements on the micro-distribution of chemical elements present in the deposits of floating plastics. Major findings were the diffusion of the ion Cl^- in the polymer matrix and the determination of the depth structure of biotic and sedimentary deposits on PET and HDPE polymers. The absorption of elements such as Cl by the polymer and the deposition of sedimentary materials may have consequences in plastic degradation speed, transference of metals and contaminants and in their toxicity to aquatic life. Combining both transversal and surface analysis can be a good exploratory strategy to assess matrix penetration profiles and depth structure of abiotic and biotic deposits on plastic materials. Although assessing the polymer-deposit interaction and matrix changes was not straightforward, the depth structure of the deposit can be well defined as long as the RBS spectra can be well modelled. In these cases sub-micrometre depth resolution can be achieved. The results of the present study evidence that nuclear microscopy in combination with the OMDAQ2007 and NDF analytical tools offer unique possibilities to study plastic degradation and plastic chemical transfer with minimal sample manipulation.

There are plenty of room to improve both OMDAQ2007 and NDF depth structure assessment. A common issue will be the acquisition of spectral data with greater statistical power. This would help improving the estimation of diffusion of elements into the polymer matrix. The examination of deposits in a temporal scale perspective would also shed light on the adhesion process of materials to plastics and on the diffusion of ions present in seawater, such as Cl^-. The NDF capabilities account for roughness, voids and different layer edge configurations, which would be interesting to explore in the search of solutions that would describe more accurately the spectral data of deposits. However, NDF is a time consuming approach and convergence to an appropriate solution is not always obtained. On the other hand the OMDAQ2007 analyses, are carried out in a friendly user interface, are fast and quantitative results are not only limited to the elements present in RBS and PIXE spectra. The evaluation of multilayer depth structures is also possible, although the final solution may be only qualitative.

Acknowledgements

This thesis was financed by the Portuguese Fundaao para a Cincia e Tecnologia (FCT) through the projects PLASTICGLOBAL (PTDC/MAR-PRO/1851/2014), UID/BIO/04565/2013, UID/Multi/04349/2013, Programa Operacional Regional de Lisboa (LISBOA-01-0145-FEDER-007317) and Erasmus+ mobility programme.

Author is especially indebted to Prof. T. Pinheiro, Prof. M. T. Peña and Prof. L. C. Alves for all the help provided not only during the experimental activity at CTN and to Prof. V. Corregidor for her assistance with NDF.

References

[1] GESAMP. Sources, fate and effects of microplastics in the marine environment: a global assessment. *IMO/FAO/UNESCO-IOC/UNIDO/WMO/IAEA/UN/UNEP/UNDP Joint Group of Experts on the Scientific Aspects of Marine Environmental Protection, Report Studies GESAMP No 90*, page 96, 2015.

[2] Jake Martin, Amy Lusher, Richard C Thompson, and Audrey Morley. The deposition and accumulation of microplastics in marine sediments and bottom water from the irish continental shelf. *Scientific Reports*, 7(1):10772, 2017.

[3] Berit Gewert, Merle M Plassmann, and Matthew MacLeod. Pathways for degradation of plastic polymers floating in the marine environment. *Environmental Science: Processes & Impacts*, 17(9):1513–1521, 2015.

[4] Mikael Kedzierski, Mlanie D'Almeida, Anthony Magueresse, Adlaide Le Grand, Hlne Duval, Guy Csar, Olivier Sire, Stphane Bruzaud, and Vronique Le Tilly. Threat of plastic ageing in marine environment. adsorption/desorption of micropollutants. *Marine pollution bulletin*, 127:684–694, 2018.

[5] C Jeynes, MJ Bailey, NJ Bright, ME Christopher, GW Grime, BN Jones, VV Palitsin, and

RP Webb. "total iba"–where are we? *Nuclear Instruments and Methods in Physics Research Section B: Beam Interactions with Materials and Atoms*, 271:107–118, 2012.

[6] Yongqiang Wang and Michael Anthony Nastasi. *Handbook of modern ion beam materials analysis*. Materials Research Society Warrendale, Pennsylvania, 2009.

[7] Mark BH Breese, David N Jamieson, and Philip JC King. Materials analysis using a nuclear microprobe. *John! Wiley & Sons Ltd, Journals, Baffins Lane, Chichester, Sussex PO 19 1 UD, UK, 1996. 428*, 1996.

[8] GW Grime. The "q factor" method: quantitative micropixe analysis using rbs normalisation. *Nuclear Instruments and Methods in Physics Research Section B: Beam Interactions with Materials and Atoms*, 109:170–174, 1996.

[9] NP Barradas and C Jeynes. Advanced physics and algorithms in the iba datafurnace. *Nuclear Instruments and Methods in Physics Research Section B: Beam Interactions with Materials and Atoms*, 266(8):1875–1879, 2008.

[10] LC Alves, MBH Breese, E Alves, A Pal, MR Da Silva, MF Da Silva, and JC Soares. Micron-scale analysis of sic/sicf composites using the new lisbon nuclear microprobe. *Nuclear Instruments and Methods in Physics Research Section B: Beam Interactions with Materials and Atoms*, 161:334–338, 2000.

[11] JA Maxwell, JL Campbell, and WJ Teesdale. The guelph pixe software package. *Nuclear Instruments and Methods in Physics Research Section B: Beam Interactions with Materials and Atoms*, 43(2):218–230, 1989.

[12] LR Doolittle. Rump: Rutherford backscattering spectroscopy analysis package. *Nucl. Instrum. Methods Phys. Res., Sect. B*, 9:344, 1985.